MAGNETIC LOOPS: A COMPARISON OF EXTRAPOLATIONS FROM THE PHOTOSPHERE WITH CHROMOSPHERIC MEASUREMENTS

Thomas Wiegelmann, Andreas Lagg, Sami K. Solanki, Bernd Inhester, and Joachim Woch

Max-Planck-Institut für Sonnensystemforschung, 37191 Katlenburg-Lindau, Germany

ABSTRACT

Direct observations of chromospheric and coronal magnetic fields are difficult and usually one has to reconstruct the 3D magnetic field from photospheric measurements. The extrapolation method depends on assumptions regarding the electric current flow in the coronal plasma. Due to the low plasma beta it is justified to assume that the currents are parallel or antiparallel to the magnetic field, the so called force-free assumption. Simplifications of the in general non-linear force-free magnetic model are linear force-free and potential fields. We compare the different magnetic field models (potential, linear force-free, non-linear force-free) with the observationally inferred structure of magnetic loops in a newly developed active region. This is the first time that the reconstructed 3D-topology of the magnetic field is available to test the extrapolations. This comparison reveals that a potential field extrapolation is not suitable for a reconstruction of the magnetic field in this young, developing active region. The inclusion of field-line-parallel electric currents gives much better results. Furthermore, a non-linear force-free computation reproduces the observations better than the linear force-free approximation.

Key words: magnetic fields, corona, chromosphere, extrapolations.

1. INTRODUCTION

Modern magnetographs, e.g. the German Vacuum Tower Telescope (VTT) measure the magnetic field vector on the photosphere. Unfortunately the magnetic field in the solar corona and chromosphere is usually not measured directly, except for a few individual case, eg. Solanki et al. (2003); Lagg et al. (2004). The classical approach to derive the chromospheric and coronal magnetic field is to extrapolate the photospheric magnetic field into the solar's atmosphere. Here we compare measurements of chromospheric magnetic fields with extrapolated fields.

2. CORONAL MAGNETIC FIELD MODELS.

The magnetic pressure in the low and middle corona is much higher than the plasma pressure (small plasma β) therefore the magnetic field is nearly force-free. The extrapolation methods based on this assumption include potential field extrapolation (e.g. Semel (1967)), linear force-free field extrapolation (e.g. Chiu and Hilton (1977); Seehafer (1978)) and nonlinear force-free field extrapolation (e.g. Sakurai (1981); Amari et al. (1999); Wheatland et al. (2000); Wiegelmann (2004); Wheatland (2004); Valori et al. (2005). Force-free magnetic fields have to obey the equations

$$(\nabla \times \mathbf{B}) \times \mathbf{B} = \mathbf{0}, \quad (1)$$

$$\nabla \cdot \mathbf{B} = 0. \quad (2)$$

which are equivalent to

$$(\nabla \times \mathbf{B}) = \alpha \mathbf{B}, \quad (3)$$

$$\mathbf{B} \cdot \nabla \alpha = 0. \quad (4)$$

In general α is a function of space, which corresponds to the non-linear force-free approach. A popular simplification is to choose $\alpha = \text{constant}$ in the entire space, the linear force-free approach. A further simplification is the choice $\alpha = 0$ which corresponds to current-free potential fields. Here, we compute potential fields, linear force-free and non-linear force-free fields and compare the result with the observed magnetic loops.

2.1. Potential and linear force-free fields.

We use the method of Seehafer (1978) for calculating the linear force-free field for a given magnetogram and a given value of α. This method gives the components of the magnetic field for a semi-finite column of rectangular cross-section in terms of a Fourier series.

The observed magnetogram which covers a rectangular region extending from 0 to L_x in x and 0 to L_y in y is artificially extended onto a rectangular region covering $-L_x$

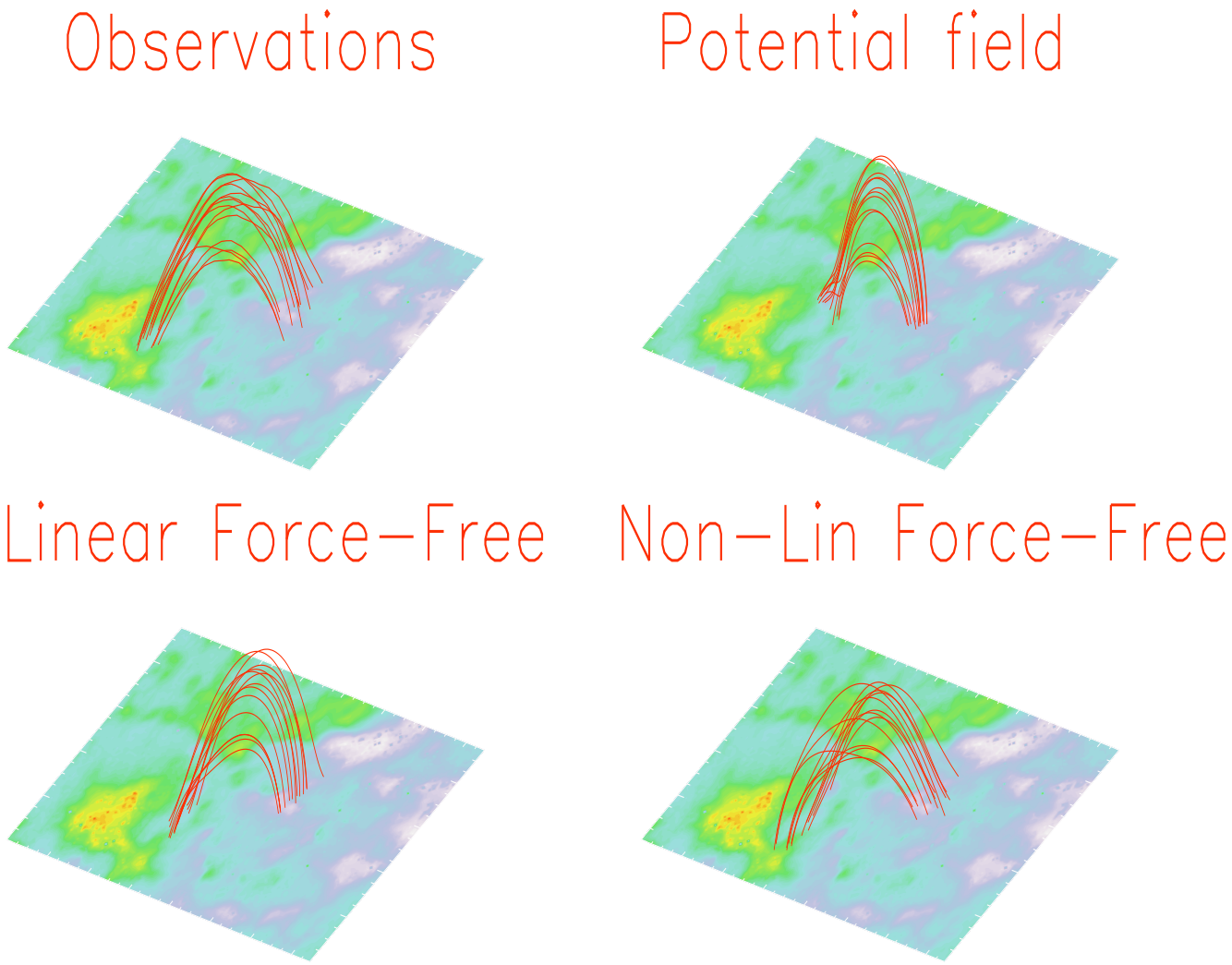

Figure 1. Observation and magnetic field extrapolations with different models.

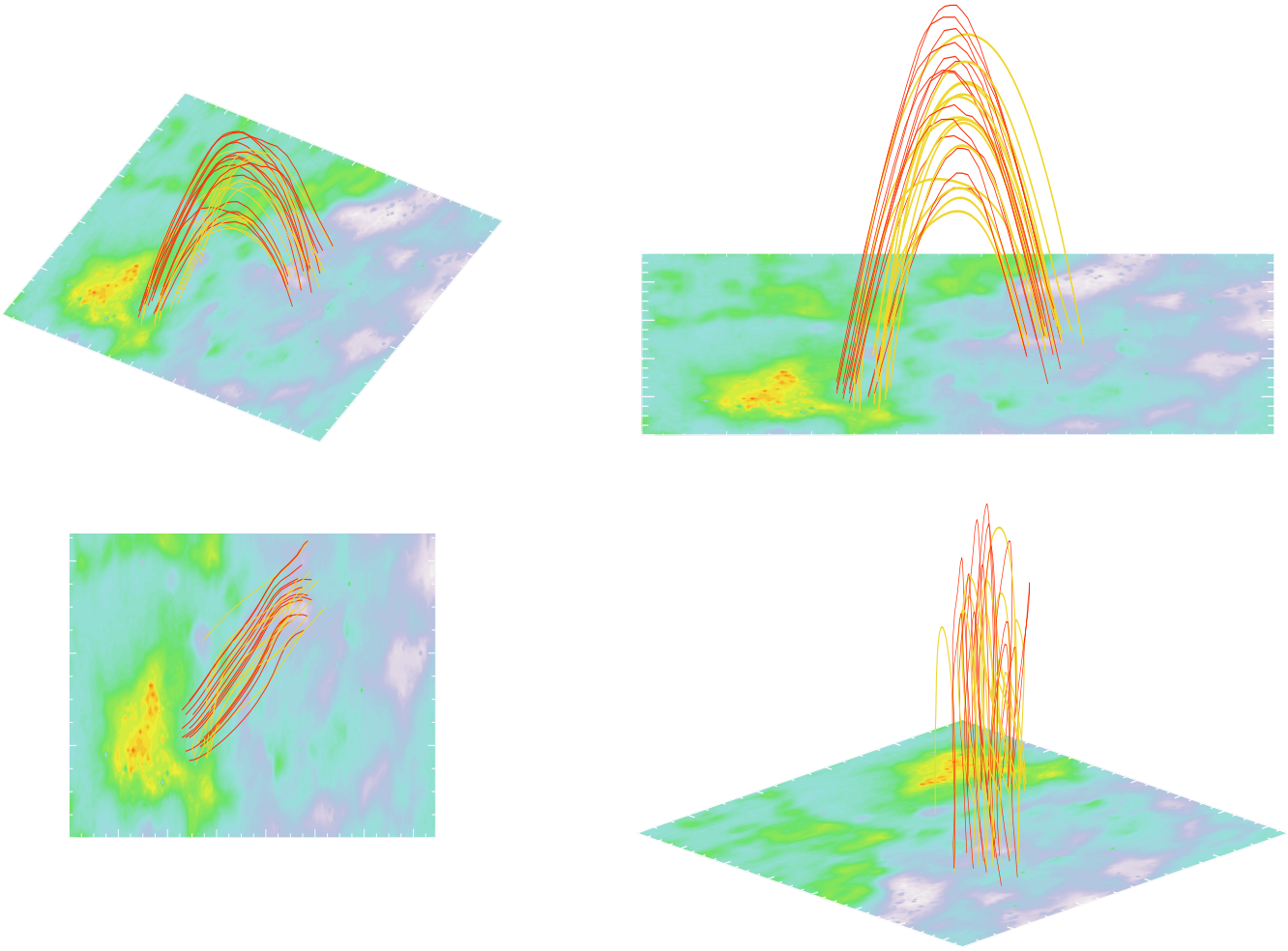

Figure 2. Observed loops (red) and non-linear force-free loops (yellow) from different viewpoints.

to L_x and $-L_y$ to L_y by taking an antisymmetric mirror image of the original magnetogram in the extended region, i.e.

$$B_z(-x,y) = -B_z(x,y) \quad (5)$$
$$B_z(x,-y) = -B_z(x,y). \quad (6)$$

The advantage of taking the antisymmetric extension of the original magnetogram is that the extended magnetogram is automatically flux balanced. The method has the further advantage that a Fast Fourier Transformation (FFT) scheme can be used to determine the coefficients of the Fourier series. For more details regarding this method see Seehafer (1978). The expression for the magnetic field is given by

$$B_x = \sum_{m,n=1}^{\infty} \frac{C_{mn}}{\lambda_{mn}} \exp\left(-r_{mn} z\right) \cdot \left[\alpha \frac{\pi n}{L_y} \sin\left(\frac{\pi m x}{L_x}\right) \cos\left(\frac{\pi n y}{L_y}\right) - r_{mn} \frac{\pi m}{L_x} \cos\left(\frac{\pi m x}{L_x}\right) \sin\left(\frac{\pi n y}{L_y}\right)\right] \quad (7)$$

$$B_y = -\sum_{m,n=1}^{\infty} \frac{C_{mn}}{\lambda_{mn}} \exp\left(-r_{mn} z\right) \cdot \left[\alpha \frac{\pi m}{L_x} \cos\left(\frac{\pi m x}{L_x}\right) \sin\left(\frac{\pi n y}{L_y}\right) + r_{mn} \frac{\pi n}{L_y} \sin\left(\frac{\pi m x}{L_x}\right) \cos\left(\frac{\pi n y}{L_y}\right)\right] \quad (8)$$

$$B_z = \sum_{m,n=1}^{\infty} C_{mn} \exp\left(-r_{mn} z\right) \cdot \sin\left(\frac{\pi m x}{L_x}\right) \sin\left(\frac{\pi n y}{L_y}\right) \quad (9)$$

with $\lambda_{mn} = \pi^2(m^2/L_x^2 + n^2/L_y^2)$ and $r_{mn} = \sqrt{\lambda_{mn} - \alpha^2}$.

The coefficients C_{mn} are obtained by comparing Equation (9) for $z = 0$ with a FFT of the magnetogram data.

To normalize α we choose the harmonic mean L of L_x and L_y defined by $\frac{1}{L^2} = \frac{1}{2}\left(\frac{1}{L_x^2} + \frac{1}{L_y^2}\right)$. The Seehafer solution contains the force-free parameter α. The force-free parameter is limited by $-\sqrt{2}\pi < \alpha L < \sqrt{2}\pi$. (See Seehafer (1978) for details.)

2.2. Non-linear force-free fields.

We solve the equations (1) and (2) by means of an optimization principle Wheatland et al. (2000); Wiegelmann (2004):

$$L = \int_V w(x,y,z) \left[B^{-2} \left|(\nabla \times \mathbf{B}) \times \mathbf{B}\right|^2 + \left|\nabla \cdot \mathbf{B}\right|^2\right] d^3x, \quad (10)$$

where $w(x,y,z)$ is a weighting function. It is obvious that (for $w > 0$) the force-free equations (1-2) are fulfilled when L equals zero. We minimize the functional (10) with an iterative scheme:

$$\frac{\partial \mathbf{B}}{\partial t} = \mu \tilde{\mathbf{F}}, \quad (11)$$

$$\tilde{\mathbf{F}} = w\,\mathbf{F} + (\mathbf{\Omega_a} \times \mathbf{B}) \times \nabla w + (\mathbf{\Omega_b} \cdot \mathbf{B}) \nabla w \quad (12)$$

$$\mathbf{F} = \nabla \times (\mathbf{\Omega_a} \times \mathbf{B}) - \mathbf{\Omega_a} \times (\nabla \times \mathbf{B}) + \nabla(\mathbf{\Omega_b} \cdot \mathbf{B}) - \mathbf{\Omega_b}(\nabla \cdot \mathbf{B}) + (\mathbf{\Omega_a^2} + \mathbf{\Omega_b^2})\,\mathbf{B} \quad (13)$$

$$\mathbf{\Omega_a} = B^{-2} (\nabla \times \mathbf{B}) \times \mathbf{B} \quad (14)$$
$$\mathbf{\Omega_b} = B^{-2} (\nabla \cdot \mathbf{B})\, \mathbf{B}. \quad (15)$$

The iterative scheme (11) ensures (for $\mu > 0$) that L is monotonically decreasing. The method works as follows:

1. Compute a potential field in the computational box.
2. Replace the bottom boundary with the observed vector magnetogramm.
3. Minimize the functional (10) with the help of Eq. (11). The continuous form of (11) guaranties a monotonically decreasing L. This is as well ensured in the discretized form if the iteration step dt is sufficiently small. The code checks if $L(t+dt) < L(t)$ after each time step. If the condition is not fulfilled, the iteration step is repeated with dt reduced by a factor of 2. After each successful iteration step we increase dt slowly by a factor of 1.01 to allow the time step to become as large as possible with respect to the stability condition.
4. The iteration stops if L becomes stationary. Stationarity is assumed if $\frac{\partial L}{\partial t}/L < 1.0 \cdot 10^{-4}$ for 100 consecutive iteration steps.

The program is written in C and has been parallelized with OpenMP. (See Wiegelmann (2004) for details.)

3. MEASUREMENTS OF MAGNETIC LOOPS IN THE UPPER CHROMOSPHERE

Complimentary to extrapolations from the photosphere, we discuss here measurements of the chromospheric magnetic field. The measurement of the magnetic field direction is based on an inversion technique applied to spectropolarimetric data of the photospheric Si I line at 1082.7 nm and the chromospheric He I 1083 nm triplet. The data were recorded with the Tenerife Infrared Polarimeter mounted on the German Vacuum Tower Telescope (VTT). The inclination and azimuthal angle from

the chromospheric magnetic field map was used to trace magnetic field lines. We identified field lines as magnetic loops if the following criteria were fulfilled: the magnetic field strength must decrease with height, the inclination and azimuthal angles must not vary strongly from one pixel to the other and the height of the two footpoints must be similar. For a more detailed description of the observations and the analysis technique we refer to Lagg et al. (2004) and Solanki et al. (2003).

4. COMPARISON OF OBSERVED AND EXTRAPOLATED LOOPS

From the 3D magnetic field models, we compute magnetic field lines with the help of a fourth order Runge-Kutta field-line tracer. The field-line tracer starts the integration at any arbitrary point in space and traces the magnetic field in $+B$ and $-B$ direction until the photosphere is reached in both directions. For a comparison with the observed loops, the integration start-points are located on the observed loop structures.

Fig. 1 shows 14 observed loops and corresponding loops from a potential, linear and non-linear force free magnetic field model. The inspection of Fig. 1 reveals that potential fields do not agree with the observations. The linear force-free approach is better, but not as good as the non-linear force-free model. In the following, we compare the different magnetic field models with the observed loops quantitatively. As a measure of how well the magnetic field lines and the observed loops agree, we compute the spatial distance of the two curves in 3D integrated along the whole loop length l from $\tau = 0$ to $\tau = l$. As a result we get a dimensionless number $C = \frac{1}{l^2}\int_0^l \sqrt{(\mathbf{r}_{\rm obs}(\tau) - \mathbf{r}_{\rm extrapol}(\tau))^2}d\tau$, where τ is the geometrical length measured along the loop and $C = 0$ if both curves coincide. For details of the comparison method and values of C for the individual loops see Wiegelmann et al. (2005). The average values of C are given in Tab. 1. As lower the value of C as better observed and reconstructed loops agree. The quantitative comparison shows that we get the best agreement of observations and model for a non-linear force-free approach. The linear force-free model is worse then the non-linear one, but significantly better than potential fields. We show a comparison of the observed loops (in red) and non-linear force-free loops in Fig. 2 from different viewpoints. There is certainly no perfect alignment, but the overall structure of the magnetic field is very similar.

Table 1. Quantitative comparison (average value of C) of the observed loops with different magnetic field models for the 14 loops shown in Fig. 1 and Fig. 2.

Model	average C	Standard deviation
Potential field	0.52	± 0.09
Linear force-free	0.33	± 0.04
Non-linear force-free	0.21	± 0.06

5. CONCLUSIONS

We compared direct observations of magnetic loops in the upper chromosphere with the magnetic field extrapolated from the photosphere with different models. The simplest model, a potential field, does not reproduce the observations. A linear force-free model provided better significantly better results and the shear of the loops seems to be described approximately correct within this approach. The most involved model used here, a non-linear force-free approach provided the best results. Let us remark that the computation of non-linear force-free fields is more challenging because of the intrinsic non-linearity of the underlying mathematical problem. A further complication is, that this model requires photospheric vector magnetograms as input, which have ambiguities and high noise in the transversal photospheric magnetic field component. Current vector magnetographs have also a limited field of view and data are not available for many regions. This limitation will vanish, however, in the nearest future as soon as data from the full disc vectormagnetograph SOLIS (Synoptic Optical Long-term Investigations of the Sun, U.S. National Solar Observatory, Kitt Peak) become available. The mathematical difficulty as well as the lack of data from vectormagnetographs explain the popularity of potential and linear force-free models. This study revealed, however, that a non-linear force-free approach is necessary to describe the magnetic field in active regions accurately. Furthermore a known limitation of linear force-free models Seehafer (1978) is that they cannot be used to compute the magnetic energy, because within this model the magnetic energy is unbounded in the half space above the photosphere. As the free magnetic energy in active regions is supposed to play an important role for the occurrence of eruptive phenomena, e.g. flares and coronal mass ejections, it is important to compute this quantity accurately with help of a non-linear force-free approach.

ACKNOWLEDGMENTS

We acknowledge the use of data from the German VTT. The work of T. Wiegelmann was supported by DLR-grant 50 OC 0007.

REFERENCES

Amari, T., Boulmezaoud, T. Z., Mikic, Z.: 1999, A&A, 350, 1051.

Chiu, Y.T., Hilton, H.H.: 1977, ApJ, 212, 821.

Lagg, A., Woch, J., Krupp, N., Solanki, S.K.: 2004, A&A, 414, 1109.

Sakurai, T.: 1981, Sol. Phys., 69, 343.

Seehafer, N.: 1978, Sol. Phys., 58, 215.

Semel, M.: 1967, Ann. Astrophys. ,30, 513.

Solanki, S.K., Lagg, A., Woch, J., Krupp, N., Collados, M.: 2003, Nature, 425, 692.

Valori, G., Kliem, B., & Keppens, R. 2005, A&A, 433, 335

Wheatland, M. S., Sturrock, P. A., Roumeliotis, G.: 2000, ApJ., 540, 1150.

Wheatland, M. S. 2004, Sol. Phys., 222, 247

Wiegelmann, T. 2004, Sol. Phys., 219, 87.

Wiegelmann, T., Lagg, A., Solanki, S. K., Inhester, B., & Woch, J. 2005, A&A, 433, 701